Induction Motor Fault Diagnosis Using a Hilbert-Park Lissajou's Curve Analysis and Neural Network-Based Decision

Samira Bensalem, Khmais Bacha, Mohamed Benbouzid, Abdelkader Chaari

Abstract – *In this work we propose an original fault signature based on the Hilbert-Park Lissajou's curve analysis. The performances of the proposed signature were compared to those of the Park Lissajou's curve which is the signature most recently used. The proposed fault signature does not require a long temporal recording, and their processing is simple. This analysis offers an easy interpretation to conclude on the induction motor condition and its voltage supply state. The proposed signature shows its efficiency especially in the case of unloaded machine. The geometrical characteristic of all Hilbert-Park Lissajou's curves are calculated in order to develop the input vector necessary for the pattern recognition tools based on neural network approach with an aim of classifying automatically the various states of the induction motor. This approach was applied to a 1.1 kw induction motor under normal operation and with the following faults: unbalanced voltage, air-gap eccentricity and outer raceway bearing defect.*

Keywords*: Induction Motor Fault Diagnosis, Lissajous Curve Analysis, Neural Network*

Nomenclature

$A(t)$	The amplitude modulation
$\psi(t)$	The instantaneous phase
$\Phi(t)$	The phase modulation
$\omega(t)$	The instantaneous pulsation
$x(t)$	The modulated signal
$H(x(t))$	The Hilbert transform
L_p	The edge length of Hilbert-Park Lissajou's curve
μ_p	The triangle mass center
$\Delta\mu$	The distance between the two mass centers
MSE	The mean square error
MLP	The multi-layer perceptron
MCSA	Motor current signature analysis

I. Introduction

Induction motors are nowadays extensively used in all types of industry applications due to their simple construction, reliability, and the availability of power converters using efficient control strategies. In this way, early fault detection and diagnosis allow preventative and condition-based maintenance to be arranged for the electrical machines during scheduled downtimes and prevent an extended period of breakdown due to extensive system failures.

For the fault detection problem, it is interesting to know if a fault exists in the system via online measurements [1].

Although induction machines are failures subjected which are inherent to the machine itself or due to external environment.

The origins of inherent failures are due to the mechanical or electrical forces acting in the machine enclosure. Researchers have studied a variety of machine faults, such as winding faults [2], broken rotor bars [3], eccentricity [4], and bearing faults [5].

Various methods for induction motor fault detection have been reported in the literature. In [6], an online induction motor diagnosis system using motor current signature analysis (MCSA) with advanced signal processing algorithms is proposed. In [7], authors propose a method based on monitoring certain statistical parameters estimated from the analysis of the steady state stator current. The approach is based on the extraction of the signal envelop by Hilbert transformation, pre-multiplied by a Tukey window to avoid transient distortion. In [8], authors use a sliding window constructed by Hilbert transform of one current phase and the fault severity is diagnosed by motor current signature analysis (MCSA) of the stored Hilbert transform of several periods.

The majority of signatures proposed in the literature are based on the signal processing tools and more particularly the fast Fourier transform (FFT), the wavelet transform [9] and the time-frequency approach (spectrogram, Wigner-Ville distribution) [10]. These signatures may cause a delay in fault detection which can cause considerable damage or even catastrophic. Indeed, the FFT requires a long recording time of the in order to guarantee a precision to detect the frequencies sensitive to defects.

In addition, the programs compilations of advanced signal processing tools (time-frequency approach, wavelet…) are slow and consume additional time.

The time lost during the recording and processing is very valuable in detecting and diagnosing faults.

The fault signatures based on the pattern analysis, especially the Lissajou's curves, are much less time consuming than those mentioned above. The Park vector pattern is the Lissajous curves the most exploited in induction motor fault diagnosis. This signature was used for detecting the following faults: unbalanced voltage [11], broken rotor bars, air-gap eccentricity [4] and the bearing failure [12].

The reference Park Lissajou's curve corresponding on the supposed healthy motor differs slightly from the expected circular one, because the supply voltage is not exactly sinusoidal. The occurrence of a voltage unbalance or an open phase manifests itself in the deformation of the Park Lissajou's curve corresponding on a healthy condition. This deformation leads to an elliptic pattern whose major axis orientation is associated to the faulty phase; this ellipse given by the Park Lissajou's curve does not evaluate the fault severity.

In the case of air-gap eccentricity, the bearing fault and the broken rotor bars, the thickness of the Park Lissajou's curve was increased. These faults have the same influence on the Park Lissajou's curve, this may cause a false fault location, where wrong diagnosis.

In this case the Park Lissajou's curve can only detect a fault occurring, but it did not identify.

In this work, our aim is to develop a fault signature based on Lissajous curve, which requires a short recording time and a simple processing; this allows us to gain valuable time. In addition the signature must detect and identify the fault and estimate its severity.

In this way, we suggest an original fault signature based on the pattern analysis using an improved combination of Hilbert and Park transforms. The geometrical characteristic of all patterns are calculated in order to develop the input vector necessary for the pattern recognition tool based on neural network approach with an aim of classifying automatically the various states of the induction motor. This approach was applied to a 1.1 kW induction motor under normal operation and with the following faults: unbalanced voltage, air-gap eccentricity and outer raceway bearing defect.

II. Basic Theory of the Proposed Fault Signature

The basic idea is instead of using directly the three lines currents to calculate the park vector, we only employ useful information immersed in these currents.

For this reason we apply the Hilbert transform to the three line currents. Indeed Hilbert transform is used to acquire the instantaneous frequency and instantaneous amplitude. It reveals modulation in signals caused by faulty components. In addition, it removes carrier signals and this will reduce the influence of irrelevant information for the purpose of fault detection. Fig. 1 illustrates the block diagram of the proposed induction motor fault diagnosis methodology. The development of our fault signature requires initially the calculation of the modulus and the phase of the Hilbert transform of each three currents.

Thereafter we apply the Park transform to the three phases and three modulus. After the Park transform, we can draw the two Lissajous curves relating to the modulus and the phase. In the continuation, we will present the principal concepts of the Hilbert and Park transforms.

II.1. Demodulations by Hilbert Transform

The demodulation consists in extracting from the signal, the functions of phase and amplitude modulation.

The frequency and amplitude modulation can be expressed as:

$$x(t) = A(t)\sin\psi(t) \tag{1}$$

where $A(t)$ expresses the amplitude modulation and $\psi(t)$ expresses the instantaneous phase.

The instantaneous phase $\psi(t)$ is expressed as:

$$\psi(t) = \omega t + \Phi(t) \tag{2}$$

where $\Phi(t)$ expresses the phase modulation.

The instantaneous pulsation of the signal ω_{inst} is equal to derived from the instantaneous phase:

$$\omega_{inst} = \frac{d}{dt}\left(\psi(t)\right) = \omega + \frac{d}{dt}\left(\Phi(t)\right) \tag{3}$$

The equation $x(t)$ of a modulated signal is expressed as:

$$x(t) = A(t)\sin\left(\omega t + \Phi(t)\right) \tag{4}$$

We can form an analytical signal while adding to the modulated signal $x(t)$, the Hilbert transform $H(x(t))$ in his imaginary part:

$$\tilde{x}(t) = x(t) + iH\left(x(t)\right) \tag{5}$$

The Hilbert transform is expressed as:

$$H\left(x(t)\right) = \frac{1}{\pi}\int_{-\infty}^{+\infty} x(\tau)\frac{1}{1-\tau}d\tau \tag{6}$$

In other way, the Hilbert transform corresponds to the Convolution of $x(t)$ by $1/\pi\tau$:

$$H\left(x(t)\right) = x(t) * 1/\pi\tau \tag{7}$$

where * is the convolution indicate.

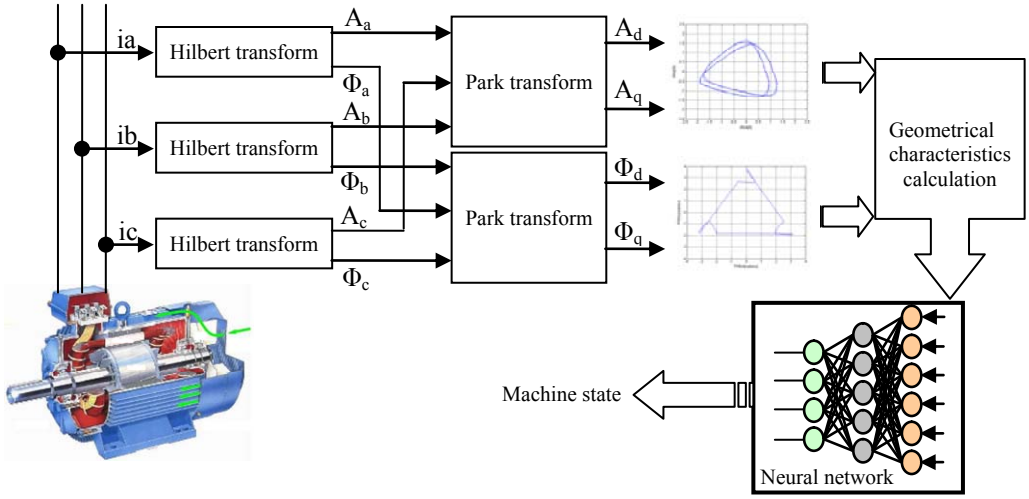

Fig. 1. The proposed methodology for induction motor fault diagnosis

The function of amplitude modulation $A(t)$ (amplitude of the envelop) is expressed as:

$$A(t) = \sqrt{x^2(t) + H^2(x(t))} \tag{8}$$

The function of phase modulation $\Phi(t)$ (instantaneous phase) is expressed as:

$$\Phi(t) = tan^{-1}\left(\frac{H(x(t))}{x(t)}\right) \tag{9}$$

The instantaneous pulsation $\omega(t)$ becomes (in rad/s):

$$\omega(t) = \omega + \frac{d}{dt}(\Phi(t)) \tag{10}$$

The Hilbert function of the $H(x(t)$ *signal*) thus makes it possible to calculate the functions of phase and amplitude modulation as well as the instantaneous frequency by using the equations of $A(t)$, $\Phi(t)$ and $\omega(t)$.

The demodulation is a very powerful tool to detect any defect which causes the modulation of the signal.

II.2. Park Transform

The Park transform consists in passing from a three-phase system to a two-phase system.

A two-dimensional representation can then be used for describing three-phase induction motor phenomena; a suitable one is being based on the Park's vector.

As a function of mains phase variables (x_a; x_b; x_c) the Park's vector components (x_d; x_q) are:

$$x_d(t) = \sqrt{\frac{2}{3}}x(t) - \frac{1}{\sqrt{6}}x_b(t) - \frac{1}{\sqrt{6}}x_c(t) \tag{11}$$

$$x_q(t) = \frac{1}{\sqrt{2}}x_b(t) - \frac{1}{\sqrt{2}}x_c(t) \tag{12}$$

III. Experimental Results

III.1. Test Bench Description

The test motor used in the experimental investigation has been a three-phase 50-Hz, 28 rotor bars, four-pole, 1.1-kW induction machine (Fig. 2(a)). The induction machine shaft is mounted with a powder brake in order to simulate different level of load torque during the tests (0%, 20%, 40%, 60%, 80% and 100% of full loaded torque). The studied faults are: unbalanced voltage, air-gap eccentricity and the outer raceway bearing defect.

The first one, stator voltages have been unbalanced by adding a resistance to one phase. The created unbalanced voltage ratios are: 15%, 10%, 5% and 3%.

In order to create an air-gap eccentricity fault in the induction motor, a simple mechanism has been used. Each of the two bearing housings of the rotor has been changed to a pair of eccentric rings placed one into the other (Fig. 2(b)). The defective bearings have been installed on the load side of the induction motor. The diagnosis of bearing failures on the load side of the mechanics succeeds as well. The generated artificial faults that have been installed for the following results are shown in Fig. 2(c) for the outer raceway bearing fault. Eroding the ring of the bearing has resulted in a slot with a width of 5 mm at the outer raceway. The investigated bearing contains 9 balls. Three phase current sensors are used to monitor the induction machine while working at steady state. Low-pass anti-aliasing filters are implemented in order to set the frequency bandwidth of the analysed signals to a correct range. Then, the outputs of the low-pass filters are directly connected to a data acquisition board (dSpace DS1104 processor board) which contains a Motorola Power PC 603e model and a DSP (TMS320F240 – 20 MHz).

The process can be commanded and monitored via the Control Desk software of dSpace. The data sampling is performed using differential channels and a sampling frequency is 10 kHz. The software used is MATLAB™ for the data acquisition and processing.

(a)

(b)

(c)

Figs. 2. Experimental set-up of 1.1 kW to collect healthy and faulty induction machine data in stator current

III.2. Hilbert-Park Lissajous Curves Analysis

The motor has been initially tested in healthy condition, in order to verify Hilbert-Park Lissajou's reference curve. Fig. 3 and Fig. 4 show respectively the typical Hilbert modulus-Park Lissajou's curve and the Hilbert phase-Park Lissajou's curve corresponding to a healthy motor. We can consider the two patterns are similar to equilateral triangles. We can deduce that the mass centers for the Hilbert modulus-Park (Fig. 3) and for the Hilbert phase-Park Lissajou's curves (Fig. 4) are located at the origin (0, 0).

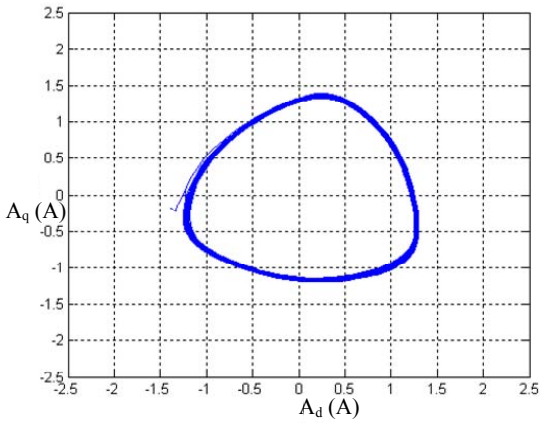

Fig. 3. Hilbert modulus-Park Lissajou's curve for fully loaded motor in normal condition

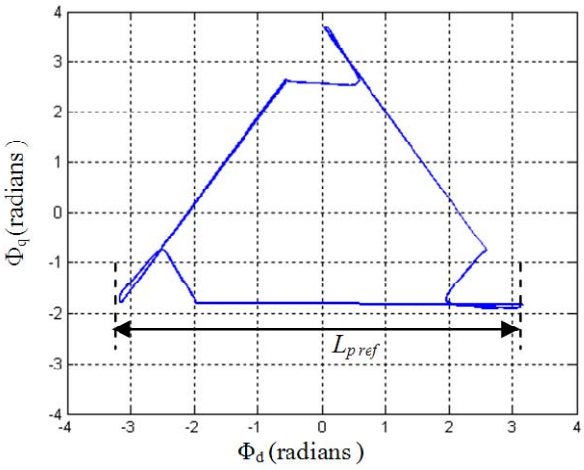

Fig. 4. Hilbert phase-Park Lissajou's curve for fully loaded motor in normal condition

Other experimental tests have carried out at different load level in normal condition which have presented in Figs. 5. We can note that the Hilbert modulus-Park Lissajou's curve keep the same form (equilateral triangle; mass center in the origin) at any level of load. But the triangle dimensions are reduced according to the load level. Concerning the Hilbert phase-Park Lissajou's curve, the variation of the load level does not influence its forms and its dimensions.

Figs. 6 show Park Lissajou's curve of the healthy motor. The curve is expected to have circular shape centred at origin.

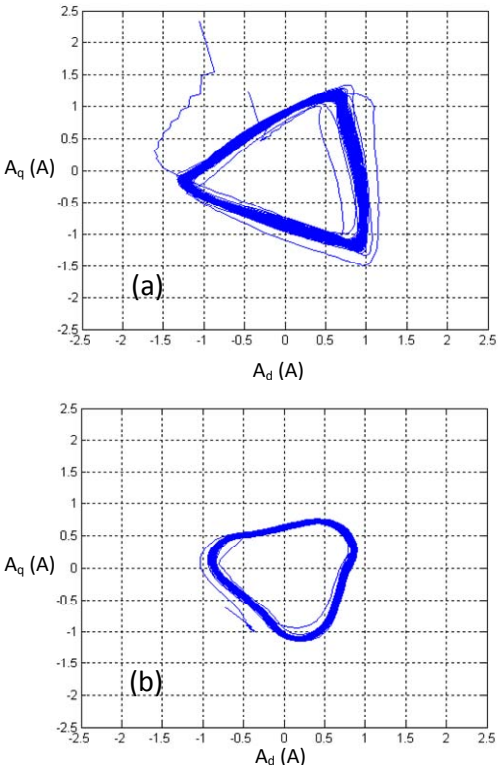

Figs. 5. Effect of the load level in the Hilbert modulus-Park Lissajou's curve for a healthy motor : (a) 60%, (b) 0%

Fig. 6(b) shows Park Lissajou's curve of the healthy unloaded motor. In this case the Lissajous curve is under great strain from the reference circle.

Afterward, three kinds of experiments have been carried out. In the first one, stator voltages have been unbalanced by adding a variable resistor to one phase in order to create several faults severity level (3%, 5%, 10% and 15% of nominal voltage). The unbalanced supply voltages are illustrated in Fig. 7.

The occurrence of a voltage unbalance manifests itself in the deformation of the Hilbert modulus-Park and the Hilbert phase-Park Lissajou's curves corresponding to a healthy condition. In Figs. 8 we can notice that the mass center corresponding to the Hilbert modulus-Park Lissajou's curve is relocated towards the negative part of the x-axis.

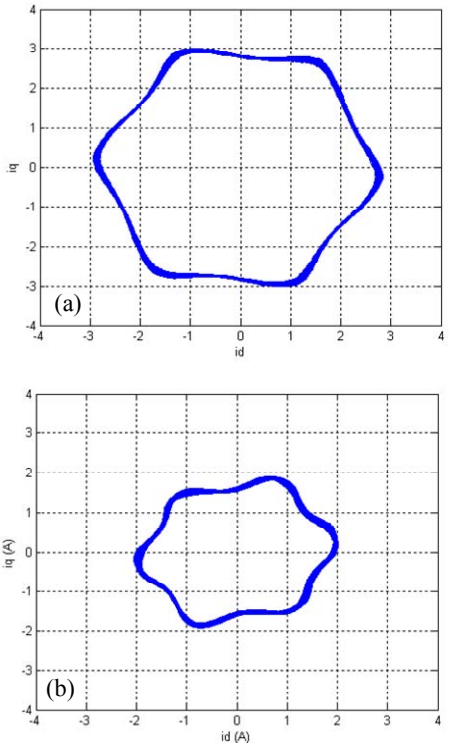

Figs. 6. Park Lissajou's curve in normal condition for : (a) fully loaded motor , (b) unloaded motor

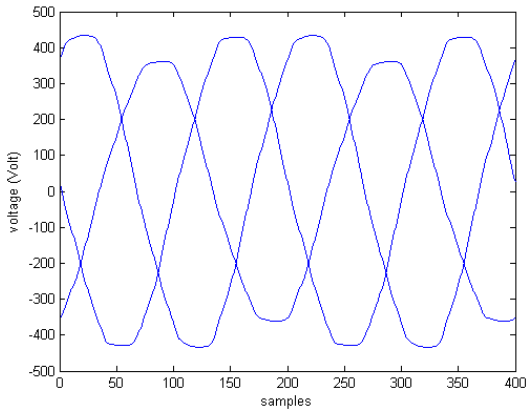

Fig. 7. Unbalanced supply voltages

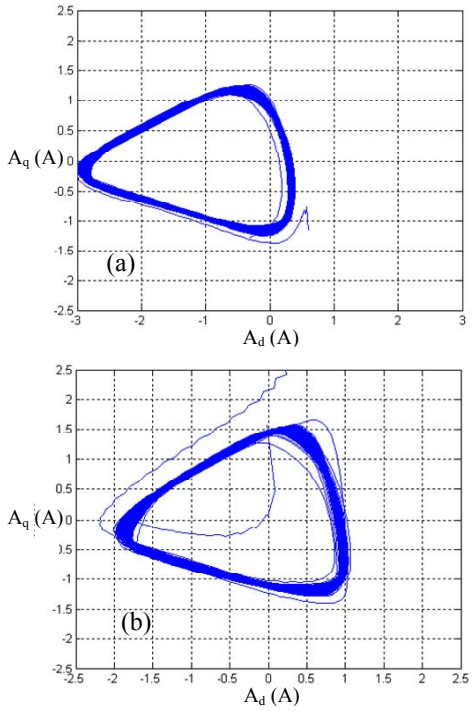

Figs. 8. Effect of stator voltage unbalance level in Hilbert modulus-Park Lissajou's curve for fully loaded motor: (a) 15%, (b) 5%

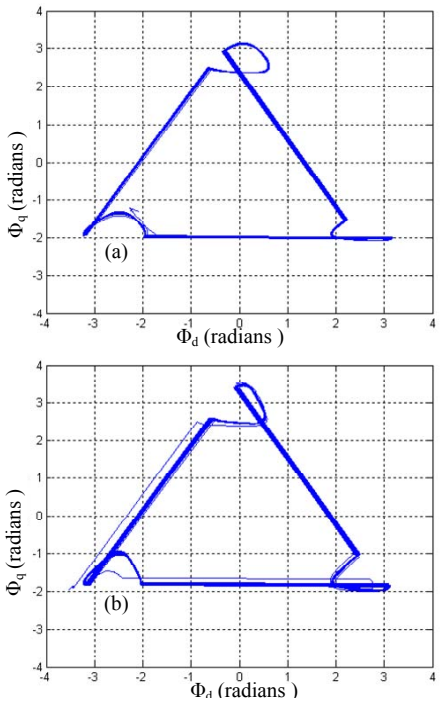

Figs. 9. Effect of stator voltage unbalance level in Hilbert phase-Park Lissajou's curve pattern for fully loaded motor: (a) 15%, (b) 5%

Concerning the Hilbert phase-Park Lissajou's curve, the mass center is relocated slightly towards the negative part of the x-axis, and one of the triangle edges length has increased (its length becomes L_p instead of $L_{p\ ref.}$), that correspond to the unbalanced phase, these deformations are illustrated in Figs. 9. Starting from the Hilbert phase-Park Lissajou's curve we can detect, locate

the unbalanced phase and estimate his severity degree, and the last one is quantified by the following relationship:

$$\frac{L_p - L_{p\,ref}}{L_{p\,ref}} \times 100 \qquad (13)$$

with $L_{p\ ref}$ is the reference edge length (in normal condition). This behaviour is checked for several fault severity degrees (Figs. 8 and Figs. 9). The gravity center displacement towards the x-axis negative part of the Hilbert modulus-Park Lissajou's pattern, and the edge length of the Hilbert phase-Park Lissajou's pattern, vary according to the fault severity. Even under operation in the low load levels, we get the same performances of detection, localization and the fault severity estimate (Figs. 10). Figs. 11 show the deformation of the Park Lissajou's curve in the occurrence of a voltage unbalance. This deformation leads to an elliptic pattern whose major axis orientation is associated to the faulty phase; this ellipse given by the Park Lissajou's curve cannot evaluate the fault severity. In the case of unloaded machine, (Fig. 11(b)) the shape is very different from the elliptical; the diagnosis is difficult and imprecise.

The second one has concerned air-gap eccentricity fault. If the Hilbert modulus-Park Lissajou's curve for a 4-pole motor is drawn over one cycle, two distinct curves are obtained under air-gap eccentricity as it is shown in Fig. 12.

This figure presents two shifted equilateral triangles. The distance between the mass centers of the two shifted triangles can be used as an index for the estimation of the air-gap eccentricity degree. Also, the noise occurrence, the rotor bar number and the motor rated power have no considerable effects on the performance of this index and it has the advantage to the simplicity of measurement and computation.

The third one is the outer raceway bearing fault. Fig. 13 illustrates two shifted triangles similar to the case of the eccentricity fault, it is completely normal because the bearing defect causes an air-gap eccentricity. The only difference is that the triangles are not equilateral but isosceles. The Hilbert phase-Park Lissajou's curve has not been modified compared to its reference.

In Figs. 14, the Park Lissajou's curves related to the air-gap eccentricity and the outer raceway bearing fault are shown. It is observed that the thicknesses of these curves are clearly increased compared to Fig. 6(a). These faults have the same influence on the Park Lissajou's curve, this may cause a false fault identification, where wrong diagnosis. In this case the Park Lissajou's curve can only detect a fault occurring, but it did not identify.

Starting from the patterns mentioned above, we can calculate the geometrical characteristics of the Hilbert modulus-Park Lissajou's curve and the Hilbert phase-Park Lissajou's curve in order to develop the input vector necessary for the pattern recognition tools based on neural network approach with an aim of classifying automatically the various states of the induction motor.

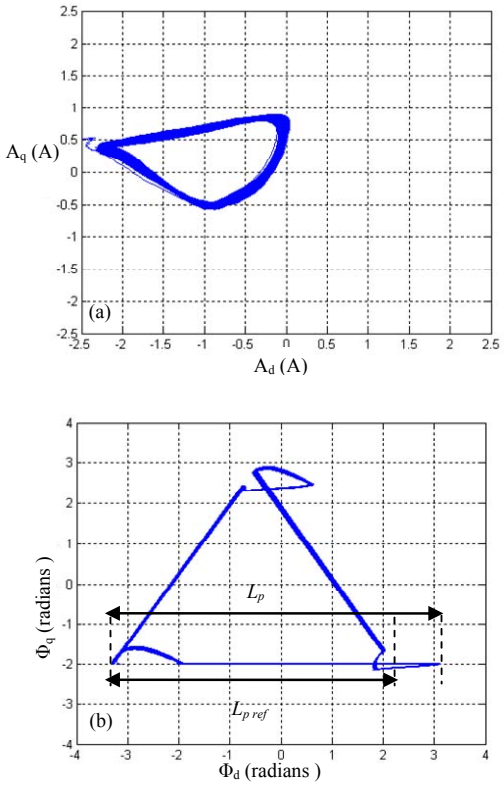

Figs. 10. 15% stator voltage unbalance in the case of 20% for fully loaded motor: (a) Hilbert modulus-Park Lissajou's curve, (b) Hilbert phase-Park Lissajou's curve

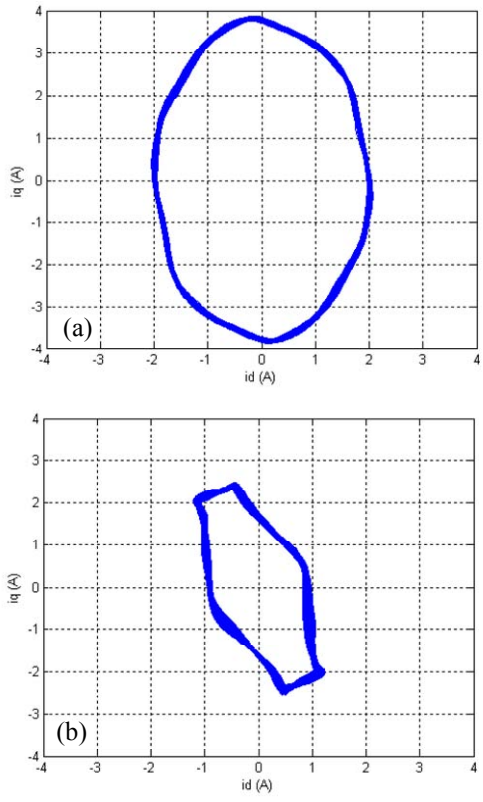

Figs. 11. Effect of stator voltage unbalance on the Park Lissajou's curve for: (a) fully loaded motor, (b) unloaded motor

III.3. Calculation of the Pattern Geometrical Characteristics and the Development of the Training Input Vector

The index presented above must be described in a numerical form. In the following, we calculate the geometrical characteristics of the Hilbert phase-Park and the Hilbert modulus-Park Lissajou's curves. Finally we get developed the input vector necessary for the neural network training.

Computation of the geometrical characteristics of the Hilbert phase-Park Lissajou's curve

200 points are quite sufficient to describe a closed Hilbert phase-Park Lissajou's curve (Fig. 15(a)). The first step consists in computing the co-ordinates of the triangle mass center $\mu_p(\mu_{px}, \mu_{py})$. The second step consists in computing the length of the three triangle edges (L_{p1}, L_{p2}, L_{p3}).

Computation of the geometrical characteristics of the Hilbert modulus-Park Lissajous pattern

The calculation of these characteristics requires 200 points (Fig. 15(b)). Initially we use only 100 points (from 1 to 100) which are necessary for the description of the first triangle. We determine the co-ordinates of the triangle mass center $\mu_{m1}(\mu_{m1x}, \mu_{m1y})$ and the three triangle edges lengths (L_{m1}, L_{m2}, L_{m3}).

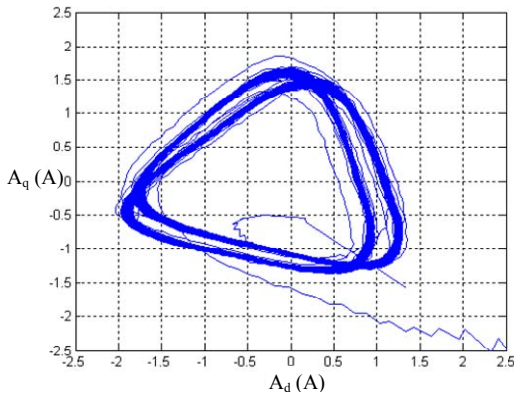

Fig. 12. Hilbert modulus-Park Lissajou's curve for fully loaded motor in the case of air-gap eccentricity fault

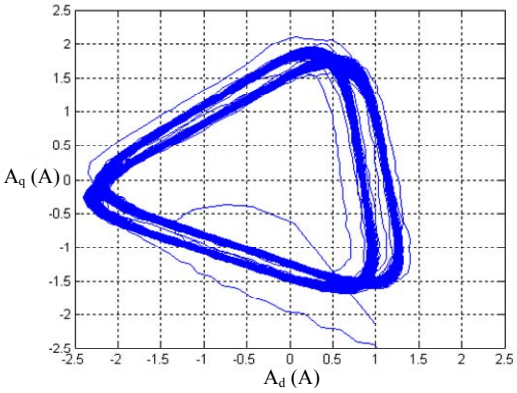

Fig. 13. Hilbert modulus-Park Lissajou's curve for fully loaded motor in the case of outer raceway bearing defect

In the second time we use the following 100 points (from 101 to 200) to draw the second triangle.

This second triangle will be shifted comparing to the first one in case of the mechanical defects (air-gap eccentricity and outer raceway bearing fault), if not, the two triangles will be confused. We determine the triangle mass center co-ordinates $\mu_{m2}(\mu_{m2x}, \mu_{m2y})$. We can calculate the distance $\Delta\mu$ (14) between the two mass centers of both triangles; it can be a good index for the mechanical fault diagnosis. With:

$$\Delta\mu = \sqrt{\left(\mu_{m1x} - \mu_{m2x}\right)^2 + \left(\mu_{m1y} - \mu_{m2y}\right)^2} \qquad (14)$$

For Hilbert phase-Park and the Hilbert modulus-Park Lissajou's curves, the determination of geometric characteristics needs only 200 points (Fig. 15). Whereas for the extraction of data (average thickness) from the Park Lissajou's curve, we used 400 points (0.04 Second = two complete cycle of line current) (Fig. 16). Our proposed signature uses only half of the points allocated for tracing the Park Lissajou's curve, which saves time during the online diagnostic.

Development of the input vector

This vector must characterize the fault signature and consequently the state of the machine. It must contain the maximum of information with a reduced size in order to have the minimum of neurons in the input layer of neural network. This vector (15) is created by the geometrical characteristics of the Hilbert modulus-Park Lissajou's curve and Hilbert phase-Park Lissajou's curve.

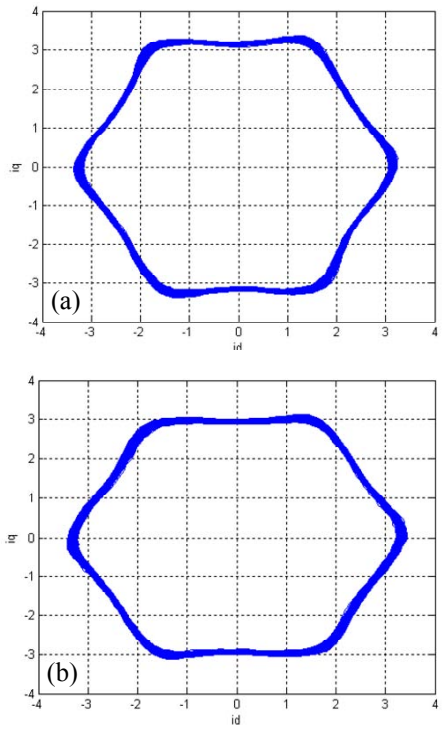

Figs. 14. Park Lissajou's curve for fully loaded motor in the case of: (a) air-gap eccentricity, (b) outer raceway bearing defect

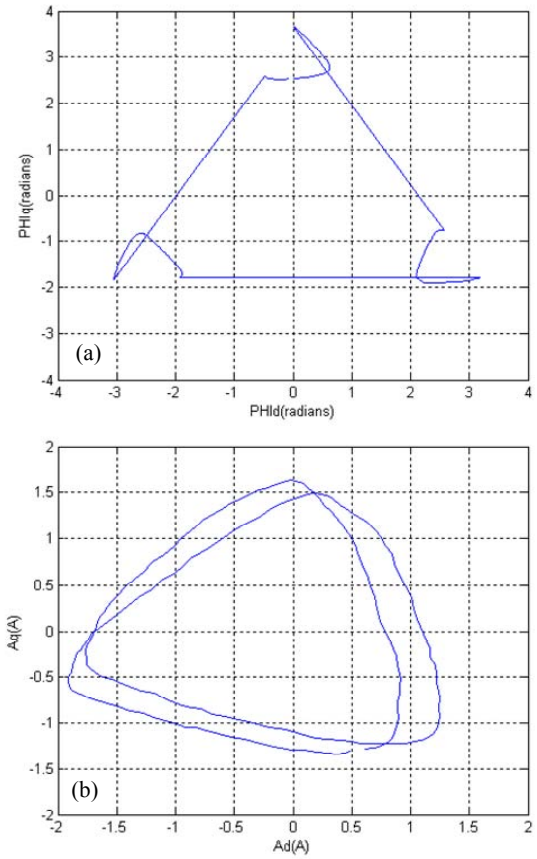

Figs. 15. (a) Hilbert phase-Park Lissajou's pattern, (b) Hilbert modulus-Park Lissajou's pattern plotted by 200 points (0.02 s)

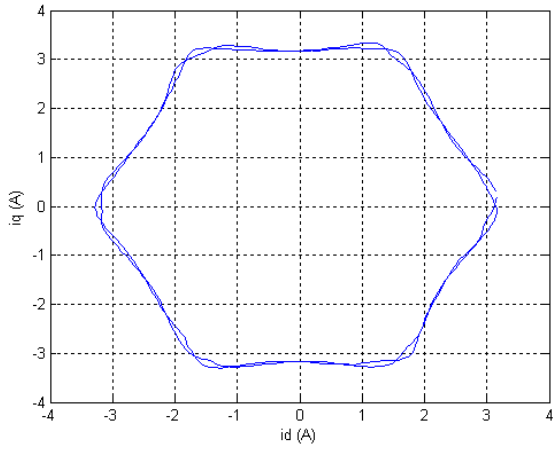

Fig. 16. Park Lissajou's curve plotted by 400 points (0.04 s)

We used the ratio between the triangles edges of the Hilbert modulus-Park Lissajou's curve in order to eliminate the influence of the various load levels (the lengths of the triangle edge depend on the load level).

We use the ratio (min/max) to have always a ratio lower than 1, which is ideal for the neural network inputs.

Concerning the coordinate of the mass centers, we keep only the X-coordinates because the shift of the triangles in case of unbalanced voltage is done along the x-axis.

$$V = \begin{bmatrix} \dfrac{min\left(L_{p1}, L_{p2}, L_{p3}\right)}{max\left(L_{p1}, L_{p2}, L_{p3}\right)} \\ \mu_{px} \\ \dfrac{min\left(L_{m1}, L_{m2}, L_{m3}\right)}{max\left(L_{m1}, L_{m2}, L_{m3}\right)} \\ min\left(\mu_{mx1}, \mu_{mx2}\right) \\ \Delta\mu \end{bmatrix} \quad (15)$$

III.4. Decision-Making Using Neural Network

In order to improve the effectiveness of the induction motor monitoring, we propose an automatic classification by using the neural networks.

Using the obtained results, the first stage in the recognition process is to create a database. It can be accomplished by analysing the Hilbert phase-Park Lissajou's curve and Hilbert modulus-Park Lissajou's curve for the classes which represent the states of the induction machine. Here, there are four possibilities examined as following:

1. Machine operating without defect and supplied by a balanced voltage,
2. Machine operating without defect and supplied by an unbalanced voltage (3%, 5%, 10% and 15%),
3. Machine operating with an air-gap eccentricity fault,
4. Machine operating with an outer raceway bearing fault.

All these situations have been tested under the load rates 0%, 20%, 40%, 60%, 80% and 100% of the rated load.

In this study, 690 samples have been dedicated for the training phase and 345 for the test phase. The neural network approach should overcome all the difficulties and the limitations due to the models of the faulted machine. The proposed network identifies the machine state through patterns obtained from several experimental examples of faulted machines.

As is well known, neural networks are parallel distributed processing units with different connection architectures and processing mechanisms. A multi-layer perceptron (MLP) structure is used and the training of several machine states is obtained tuning the connection weights of the neurons. To this aim the back propagation algorithm, that minimizes errors by the gradient descent rule, is adopted here.

This network contains two hidden layer. The first hidden layer is composed by 8 units and the second by 7 units. This choice has been kept after several experiences. The output layer is composed by 5 units: one decimal output intended for the severity estimation of the unbalanced voltage, and four binary outputs for indicated the machine state (one to indicate a normal condition and three to indicate faulty conditions).

All neuron use sigmoidal activation functions. A stop criterion of training is the number of epoch (here 500). Fig. 17 shows the results of the minimization.

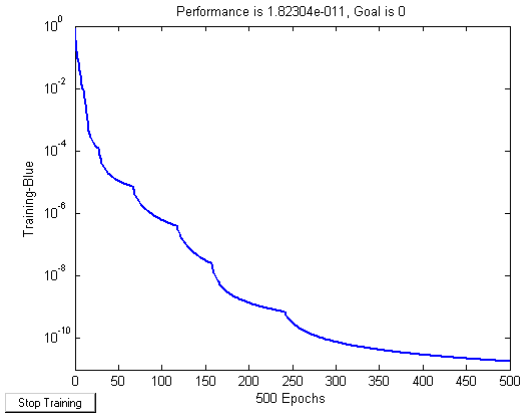

Fig. 17. The training iteration process

It can be seen that the error is very small, with means that the neural network classifies and estimate correctly the example of training set. In order to see if the network has learnt after training, the test set is again fed to the network in order to verify if it classifies and estimate correctly.

Table I shows the results by representing the false alarm and the non-detection rate of various machine states. In Table II, we can show the mean square error (MSE) of voltage unbalance evaluation. A classification rate of the fault diagnosis is 97.68%.

TABLE I
THE MLP CLASSIFICATION PERFORMANCE

	False alarm rate (%)	Non-detection rate (%)
Unbalance voltage	0 (0/345)	0.869 (3 /345)
Air-gap eccentricity fault	0.289 (1/345)	0.289 (1/345)
Outer race ball bearing fault	0.579 (2/345)	0.289 (1/345)

TABLE II
THE PERFORMANCE OF MLP SEVERITY DEGREE EVALUATION

Unbalance voltage	0%	3%	5%	10%	15%
Evaluation MSE	1.7 10^{-5}	3.88 10^{-5}	4.58 10^{-4}	4.22 10^{-4}	1.62 10^{-4}

IV. Conclusion

In this study we compared the performance of the proposed signature to those of the Park Lissajou's curve which is the signature most recently used. Concerning the eccentricity and the bearing faults, the Park Lissajou's curve only detect the occurrence of fault, but the identification and differentiation is not possible because the two faults have the same influence on the Lissajou's curve (thickness of circle).

In addition to calculate this thickness requires that the Lissajous curve course at least two cycles (0.04 seconds). Regarding the electrical faults, especially the unbalanced voltage, the extraction of parameters of the elliptical shape is difficult. This signature does not allow the estimation of the unbalanced voltage severity. In the case of unloaded machine, fault detection will be difficult because the shape of the Lissajou's curve loses its circular or elliptical. About our signature, it allows the diagnosis of unbalanced voltages and its severity in every load level. This signature also ensures the detection and identification of mechanical faults (eccentricity and bearing). The time needed to obtain the Lissajou's curve is only 0.02 Second. The proposed method has been proved to be efficient in steady state for sinusoidal power supply.

With a simple visual inspection of our fault signature, an agent of maintenance can supervise the supply voltage state and the machine condition.

In order to obtain a more robust diagnosis, it is proposed a neural network suitable to online identification of induction machine faults: unbalanced voltage, air-gap eccentricity fault and outer raceway bearing defect. The input patterns to train neural network are obtained using experimental data related to healthy and faulty machines under several load rates. The inputs of the neural network are very important for successful fault detection. In this work, we extract only the geometrical characteristics of the Hilbert modulus-Park and Hilbert modulus-Park Lissajou's patterns.

The calculation of the geometrical characteristics of the Hilbert modulus-Park and Hilbert modulus-Park Lissajou's patterns is easy and doesn't depend on the load rate. Moreover, this technique is easy to implement and uses only low-cost instruments such as three simple current sensors and a commercial data acquisition board with low resolution.

References

[1] M.-Y.Chow, Guest editorial special section on motor fault detection and diagnosis, *IEEE Trans. Ind. Electron*. 47 (5) (2000) 982-983.

[2] Rasool Sharifi, Mohammad Ebrahimi, Detection of stator winding faults in induction motors using three-phase current monitoring, *ISA Trans*. 50 (2011) 14–20.

[3] Mohammad Rezazadeh Mehrjou, Norman Mariun, Mohammad Hamiruce Marhaban, Norhisam Misron, Rotor fault condition monitoring techniques for squirrel-cage induction machine—A review, *Mech. Syst. Signal Process*. 25 (2011) 2827–2848.

[4] Jawad Faiz, Mansour Ojaghi, Different indexes for eccentricity faults diagnosis in three-phase squirrel-cage induction motors: A review, *Mechatronics* 19 (2009) 2–13.

[5] Jafar Zarei, Induction motors bearing fault detection using pattern recognition techniques, *Expert Syst. Appl*. 39 (2012) 68–73.

[6] Martin Blödt, Pierre Granjon, Bertrand Raison, and Gilles Rostaing, Models for bearing damage detection in induction motors using stator current monitoring, *IEEE Trans. Ind. Electron*. 55 (4) (2008) 1813-1822.

[7] Guillermo A. Jimenez, Alfredo O. Munoz, Manuel A. Duarte-Mermoud, Fault detection in induction motors using Hilbert and Wavelet transforms, *Electrical Engineering* (2007) 89, 205–220.

[8] Ilhan Aydin, Mehmet Karakose, Erhan Akin, A new method for early fault detection and diagnosis of broken rotor bars, *Energy Convers. and Manag.* 52 (2011) 1790–1799

[9] J. Cusido, L. Romeral, J.A. Ortega, A. Garcia, J.R. Riba, Wavelet and PDD as fault detection techniques, *Electric Power Systems Research* 80 (2010) 915–924.

[10] A. Lebaroud, G. Clerc, Accurate diagnosis of induction machine faults using optimal time–frequency representations, *Engineering Applications of Artificial Intelligence* 22 (2009) 815-822.

[11] Hamid Nejjari and Mohamed El Hachemi Benbouzid, Monitoring and Diagnosis of Induction Motors Electrical Faults Using a

Current Park's Vector Pattern Learning Approach, *IEEE Trans. Ind. Appl.* 36 (3), (2000), 730-735.
[12] Jafar Zarei, Javad Poshtan, An advanced Park's vectors approach for bearing fault detection, *Tribology International* 42 (2009) 213– 219.

Authors' information

Samira Ben Salem was born in Nabeul, Tunisia, in 1976. He received the B.Sc. and the M.Sc. degrees in electrical engineering, from the higher school of sciences and technology of Tunis, Tunisia, in 2000 and 2003 respectively. She is currently working toward the Ph.D. degree in induction motor mechanical fault diagnosis with the higher school of sciences and technology of Tunis in research unit : control, monitoring and reliability of the systems.

Khmais Bacha was born in Tunis, Tunisia , in 1975. He received the B.Sc., the M.Sc and the Ph.D. degrees in electrical engineering, from the higher school of sciences and technology of Tunis, Tunisia, in 1998, 2001 and 2008 respectively. Since 2004 he has been an Assistant than an Associate Professor at the Electrical Engineering Department of the national institute of applied sciences and technology (INSAT) of Tunis. His current research interests are fault diagnosis in induction machines and power transformer.

Mohamed El Hachemi Benbouzid (S'92–M'95–SM'98) was born in Batna, Algeria, in 1968. He received the B.Sc. degree in electrical engineering from the University of Batna, Batna, Algeria, in 1990, the M.Sc. and Ph.D. degrees in electrical and computer engineering from the National Polytechnic Institute of Grenoble, Grenoble, France, in 1991 and 1994, respectively, and the Habilitation à Diriger des Recherches degree from the University of Picardie "Jules Verne," Amiens, France, in 2000.
After receiving the Ph.D. degree, he joined the Professional Institute of Amiens, University of Picardie "Jules Verne," where he was an Associate Professor of electrical and computer engineering. In September 2004, he joined the University Institute of Technology (IUT) of Brest, University of Brest, Brest, France, as a Professor of electrical engineering. His main research interests and experience include analysis, design, and control of electric machines, variable-speed drives for traction, propulsion, and renewable energy applications, and fault diagnosis of electric machines.
Prof. Benbouzid is a Senior Member of the IEEE Power Engineering, Industrial Electronics, Industry Applications, Power Electronics, and Vehicular Technology Societies.

Abdelkader Chaari was born in Sfax, Tunisia, in 1957. He received the the M.Sc. and Ph.D. degrees in electrical engineering from the '' Ecole Normale Superieure de l'Enseignement Technique de Tunis (ENSET)'' Tunisia , in 1982 and 1986, respectively, and the Habilitation à Diriger des Recherches degree from the higher school of sciences and technology of Tunis, Tunisia in 2008.
Since 1982, he joined the higher school of sciences and technology of Tunis, Tunisia, (EcoleSupérieure des Sciences et Techniques de Tunis (E.S.S.T.T.)) as an assistant professor. Currently, he is a director of the research unit : control, monitoring and reliability of the systems (C3S: Commande, Surveillance etSûreté de fonctionnement des Systèmes). His main research interests are the identification and control of nonlinear systems, robust estimation and robust filtering.